Journal of Engineering Physics and Thermophysics, Vol. 78, No. 4, 2005

SIMULATION OF A CIRCULATION LAMINAR FLOW AROUND A SQUARE CAVITY WITH A MOBILE BOUNDARY AT HIGH REYNOLDS NUMBERS WITH THE USE OF VP2/3 AND THE FLUENT PACKAGE

S. A. Isaev,[a] P. A. Baranov,[a] N. A. Kudryavtsev,[a] D. A. Lysenko,[a] and A. E. Usachov[b]

UDC 532.517.2

A circulation laminar flow of an incompressible fluid around a square cavity with a mobile boundary at high Reynolds numbers has been analyzed on the basis of solution of steady-state Navier–Stokes equations by implicit factorized methods with the use of structured and nonstructured grids of different density as well as specialized (VP2/3) and universal (FLUENT) hydrodynamic packages.

The development of modern information technologies used for numerical simulation of physical-engineering processes in various industries, including power engineering and transport [1], is based on the rapid progress made in computational systems, in particular in personal computers, and on improvement of packages of applied programs.

Of course, the contribution of the first-mentioned component is predominant. Figure 1 presents the dependences of the computational speed (in megaflops) of different computers on the time of their being put into operation. As was noted in [2], the computational speed of modern supercomputers reaches 1 teraflop, and computers with an operation productivity of 10 teraflops will appear soon. It is even more important that the speed of comparatively low-cost work stations and popular personal computers reach several hundred megaflops, which makes it possible to calculate the turbulent flows occurring in practice by solving Reynolds equations and simulation of large vortices. As is seen from Fig. 1, the productivity of computational systems, presented in logarithmic coordinates, has grown linearly in the last few years. Moreover, the dependences presented in this figure for multiprocessor computers performing nonparallel operations are fairly optimistic. The point is that, at present, clusters are considered as the most economical, high-productivity computational systems. Thus, the prospects for numerical simulation seem to be fairly intriguing from the standpoint of improvement of computational means.

The achievements in the development of diagnostic and prognostic complexes based on solution of initial, master conservation equations was no less significant. The process in CFD computational hydrodynamics (including thermal physics and related branches of science) made in only several decades is comparable with the progress made in classical sciences over several centuries. This is explained by the rapid development of not only computer engineering but also mathematical models (models of turbulence, combustion, radiative heat exchange, and other processes) and effective computational methods. Not long ago (in the time of one generation: in the late 1960s–early 1970s) calculations were performed using programs written in one programming language (FORTRAN most often). These programs were brought into action on medium and large computers (of the BESM4 and BESM6 type) at centers of collective use. At that time, results were processed practically by hand. At the present industrial stage of development of the CFD [3], universal and specialized packages of applied programs represent complex, multicomponent systems that are, as a rule, written in object-oriented programming languages and have a "triad" structure: grid generator–solver–graphic interpreter of results. A program package includes cataloges of mathematical models of controlling physical processes determining the problem considered. Program packages are oriented to a definite computer base, most often to ordinary personal computers, which nonetheless, should have a large amount of memory (512 Mb and higher). The widespread use of personal computers has made program packages accessible to tens of thousands of users in all regions of the

[a]Academy of Civil Aviation, 38 Pilotov Str., St. Petersburg, 196210, Russia; email: isaev@SI3612spb.edu; [b]Prof. N. E. Zhukovskii State Scientific-Research Center "Central Aerohydrodynamics Institute," 17 Radio Str., Moscow, 107005, Russia. Translated from Inzhenerno-Fizicheskii Zhurnal, Vol. 78, No. 4, pp. 163–179, July–August, 2005. Original article submitted March 22, 2004.

1062-0125/05/7804-0799

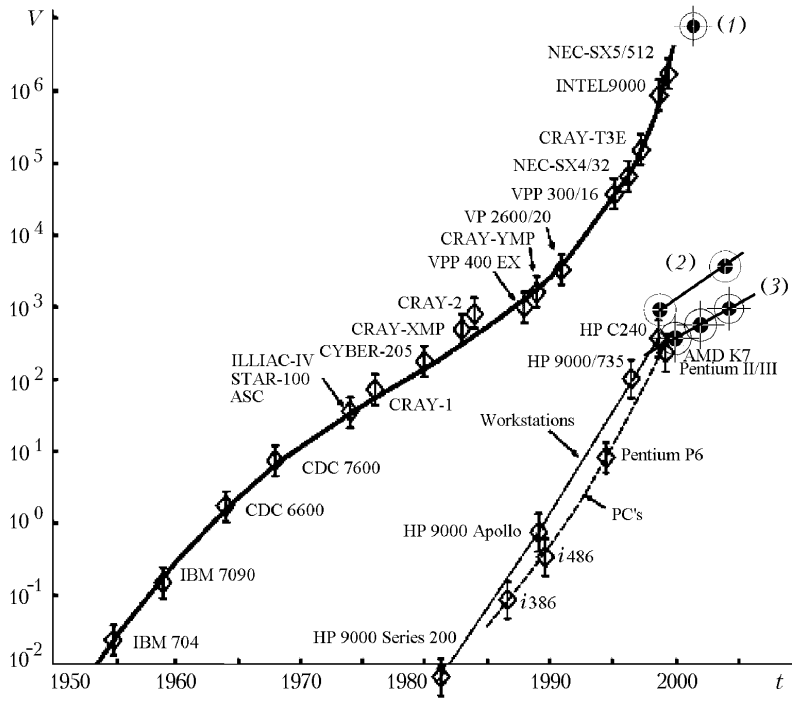

Fig. 1. Dynamics of increase in the computational speed of different-class computers [2]. Additional data: (1) Earth Simulator/NEC, $R_{max} \sim 36$ Tflops, 2002 (www.top500.org); (2) Center of Highly Efficient Cluster Technologies, St. Petersburg State Polytechnical University, $R_{max} \sim 40$ Gflops, 2003; 16 CPUs, AMD Opteron 64x, 1.8GHz; (3) Leningrad Metal-Working Plant Company, $R_{max} \sim$ G Mflops, cluster based on the Intel P4 Xeon 32x, 1.8GHz,

world. Many practical operation problems became solvable due to these program packages. However, solving complex problems with the use of program packages takes several weeks or even several months, which significantly limits the use of these packages in design works. As was already noted, one way out is by separation of computational operations and development of program packages for multiprocessor (cluster) systems. This makes it possible to increase the efficiency of solution of a problem by several times.

The widespread use of program packages creates illusions that any problems can be solved with them. One factor may be, to a large degree, the producers of these packages and the "inexperience" of purchasers (the majority of large packages are consumer), who think erroneously that program packages themselves can solve all their problems and replace expensive physical experiments. What actually happens is that the cataloges of mathematical models used in practice are not perfect and the scientific study of them is not yet finished. Moreover, the acceptability of mathematical models for solving complex problems should be specially investigated. The boundaries of applicability of the majority of models are also not clearly understood. An important problem of any numerical investigation is estimation of the adequacy of numerical forecasts. To perform this estimation it is necessary to test a package on a set of problems including model problems and problems for which there are reliable experimental data. A classical test problem is numerical simulation of a laminar flow of an incompressible viscous fluid around a square cavity with a mobile boundary. The present methodical investigation is devoted to solving the indicated problem at high Reynolds numbers with special emphasis on the comparison of results obtained using the specialized VP2/3 [4] and universal FLUENT [5] packages.

Brief Genesis of the Problem. As was noted in [6], the choice of the above-indicated test problem is not accidental. It has long since (see, e.g., [7]) been a "testing area" for approbation of approximation schemes for terms in initial equations as well as of computational models and methods. A large number of calculation data concerning this problem have been accumulated. Therefore, it makes sense to return periodically to the solution of the indicated prob-

lem at different levels of development of computer systems and software for verification and analysis of the computational complexes developed.

The interest shown by researchers in the problem on a circulation flow around a cavity was stimulated in the past by the relatively low level of computational resources required for solving it because, in this case, the computational region is limited and, therefore, a small number of grid nodes are selected and simple boundary conditions are set. For this problem, the first solutions of Navier–Stokes equations written, for economy of computational resources, in transformed vorticity–stream function variables were obtained. The calculations were performed not even on a computer but by brigades of specialists. When computers appeared, the indicated problem remained, as before, the focus of attention of specialists developing computational methods. A detailed analysis of methods concerning the problem considered that appeared in the period from the 1960s to the late 1980s is given in monographs [8, 9]. One of the authors of the present work began numerical investigation of a viscous-fluid flow around a cavity thirty years ago [10] on a BESM-4 computer containing 21×21 grid nodes in one memory cube. At that time, in the mid-1970s, high-accuracy Arakava schemes of the second and fourth order of approximation and nonuniform grids were used for the first time for solving Navier–Stokes equations. Results of parametric calculations are presented in [11] and in the textbook of L. G. Loitsyanskii [12].

One of the most important scientific achievements of the CFD in the 1980s was a numerical solution of the diffusion problem, since this problem is associated with errors in approximation of convective terms of equations. In simulation of separation flows, a necessary condition for obtaining an exact result is the use of schemes with a low numerical viscosity (upwind schemes of the second and higher orders of approximation of the type of the Leonard scheme with quadratic interpolation, the Agarval scheme, and others) [8] for representation of convective terms in transfer equations. At the same time, it has been established that the first-order schemes give erroneous solutions at high Reynolds numbers even in the case where multigrid methods are used.

Progress in computational engineering and, especially, widespread use of personal computers in the 1980s and subsequent years have made it possible, first of all, to develop universal first-wave packages of applied programs, such as the PHOENIX, FLOW3D, and FIDAP packages, and then more modern information products of the type of the FLUENT, StarCD, and CFX packages. When computers with a large memory and a high speed of response appeared, instead of the Navier–Stokes equations in transformed variables, Navier–Stokes equations written in physical variables — Cartesian velocity or pressure components — began to be predominantly used. Moreover, this made it possible to substantially (by an order of magnitude and more) increase the number of computational cells and decrease the near-wall pitches.

The range of use of program packages is wide, which is explained, first of all, by the fact that they make it possible to interpret the three-dimensional motion of inhomogeneous media in curvilinear regions of complex geometry. Program packages are predominantly used for investigating configurations of apparatus used in practice with account for their actual operating parameters. In this case, testing of packages on relatively simple problems is reduced to a minimum and is performed from case to case. At the same time, despite the availability of circumstantial guides on the use of program packages, their potentialities are not clearly understood. Such procedures as correct selection of an approximation scheme, the method of solving a problem, a grid, and scheme parameters and estimation of their influence on the solution and the convergence of results obtained with different grids are not performed in a number of cases. Investigations carried out with the use of packages accounting for the above-indicated details are few and far between. In this respect, noteworthy are two large works [13, 14], in which methodical details of solving Navier–Stokes equations at high Reynolds numbers were considered in detail. Recent numerical investigations [6, 14, 15] were devoted to analysis of the results of calculations of a circulation flow of an incompressible fluid around a square cavity at Reynolds numbers (Re) varying from 10^2 to $4 \cdot 10^4$ on grids containing as many as 200×200 cells with a minimum near-wall pitch of 10^{-4}. In the present work, in addition to the estimation of the acceptability of different program packages, we investigated flows around a square cavity in a wider range of Reynolds numbers (of up to $6 \cdot 10^4$) and verified the results of simulation of these flows with the use of finer grids (400×400 cells) that allowed us to consider the near-wall zones in detail (with a minimum near-wall pitch of up to 10^{-5}).

Comparative Analysis of Methodologies for Solving Navier–Stokes Equations with the Use of the VP2/3 and FLUENT Packages. The approach used for solving Navier–Stokes equations was developed in the 1980s. The finite-volume procedure, called the segregated procedure in the guidance for the FLUENT package [5], involves succes-

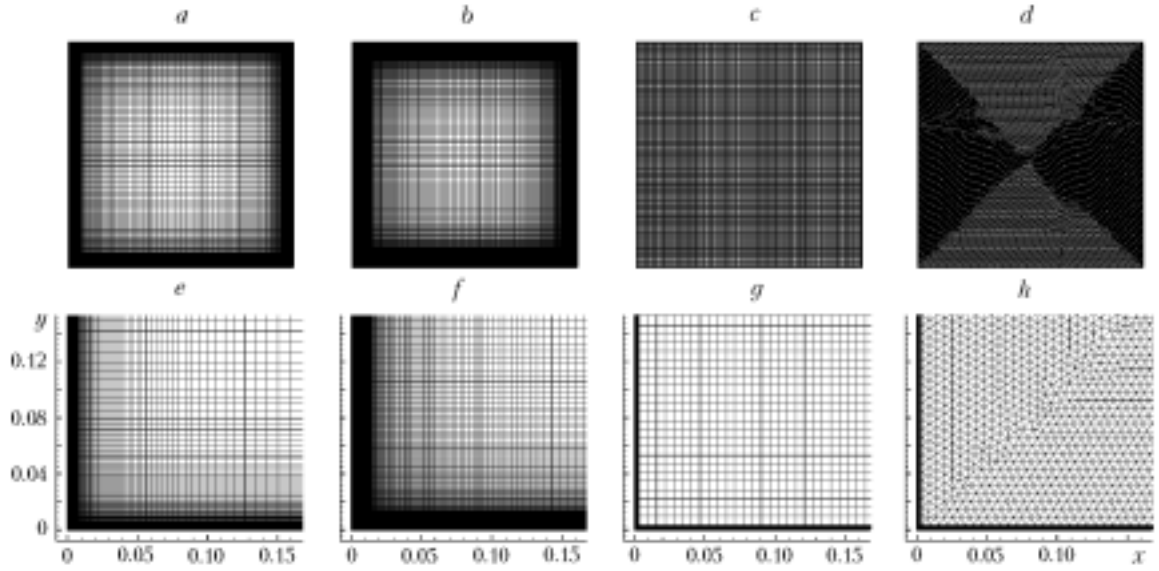

Fig. 2. Some of the selected structured (a, b, c, e, f, g) and nonstructured (d, h) nonuniform computational grids (a, b, c, d) and their fragments (e, f, g, h): a, c, d, e, g, h) 200 × 200 cells; b, f) 400 × 400 cells.

sive block-by-block solution of the system of master equations for a viscous-fluid motion. This procedure has long since been used in calculation practice [7]. Its widespread use is explained, first of all, by the fact that it is simple to formalize in a programming language and to adapt to the architecture of a computer with limited resources. It is interesting to note that, up till now, the indicated procedure has been considered as preferential in comparison to its implicit analog [5], even through the fleet of efficient computers has radically changed.

Numerical solution of the problem on fluid motion is based on separation of a computational region generated by a grid with cells of different shape. The grids are divided into structured grids — ordered grids, including rectangular ones — and nonstructured grids — predominantly triangular ones. Discretization of Navier–Stokes equations involves integration of them over the control volume of a computational cell. As a result, a system of nonlinear, algebraic vector equations is obtained. The number of these equations is equal to the number of computational cells, specifically $n \times n$ cells in the case where a structured grid is used for a square cavity (Fig. 2a). Each of the equations represents a balance equation, in which, for a homogeneous medium, nonstationary, convective, diffusion, and source terms are balanced. An important step in construction of an algorithm is linearization of equations. The commonly accepted approach (see, e.g., [5, 16]), realized in a number of universal packages, including the FLUENT package, is based on freezing of coefficients and setting of equations in terms of relative unknown dependent variables at the nodes of a computational model selected. To provide convergence in this approach it is necessary to perform additional iterations and use the lower-relaxation technique. The indicated approach was developed, first of all, for calculation of low-velocity flows (see, e.g., Patankar [17]).

Another method of linearization, based on formulation of a system of equations in increments of dependent variables, was proposed in [8] and was realized then in the original specialized VP2/3 package. This method has long been known and has effectively been used for construction of stable computational procedures (see, e.g., [18]). In [8], the indicated method was used in combination with the method of control of the calculation process, described, in part, in [19] as applied to the solution of the potential equation for transsonic flows. As a result, an efficient computational procedure of global iterations has been developed. This procedure is equally suitable for simulation of stationary and nonstationary flows of a viscous fluid; it was tested in solving three-dimensional problems on the vortex dynamics in the neighborhood of isolated holes on a plane with the use of multiblock curvilinear grids [20, 21]. It should be noted that, in the indicated works, the calculations were carried out using a working program written in the algorithmic language FORTRAN, i.e., when there were no packages of applied programs in the generally accepted sense (as they are described, e.g., in [4]).

One of the first versions of the VP2/3 package, called the UVP, had been developed for calculating a two-dimensional flow around a thick profile with vortex cells [4, 22]. In this version, a multiblock computational technology of solving problems of hydromechanics and thermal physics in multiply connected computational regions, developed in the mid-1990s, was realized. In addition to the indicated problem on a flow around a thick profile, the test problems on a laminar flow around a cylinder and the circulatory motion of a fluid in a rectangular cavity were included in the shell. The specialized package, by analogy with the universal analog, comprises a block for preparation of initial information, including a generator of grids; a solver that can control the computational process and perform its diagnostics (with a window of convergence trajectories); and an interpreter of numerical data that can process integral and experimental local characteristics as well as fields of dependent variables. Of course, the above-mentioned generator of grids in the specialized complex is designed for particular objects, even though the work with the metric is universal, i.e., such a complex is similar in many respects to the universal package. This undoubtedly holds true for the solver containing a catalog of discrete and mathematical models used for solving a much wider range of problems, as compared to the range of problems solved using the VP2/3 package. As this package became more perfect, three-dimensional nonstationary problems on the motion of inhomogeneous media and the heat exchange in them, including the heat exchange with natural convection, were included in it. Some of the methodical calculations concerning numerical investigations of laminar flows with the use of the VP2/3 package have been presented in recent works [23–26]. Among them are solutions of two-dimensional problems on a flow around a circular cylinder, including solutions in which the movement of the cylinder is taken into account (obtained with the use of sliding grids), and problems on a three-dimensional flow around a deep hole on a plane wall.

One of the most frequently used approaches to the solution of Navier–Stokes equations is the SIMPLEC method [4, 8, 9, 16]. Instead of the continuity equation, an elliptic equation for pressure correction is derived. Unlike the initial variant SIMPLE proposed by Patankar [17], the SIMPLEC variant of coordinated pressure correction, proposed by van Durmal and Reitbi, is characterized by a higher calculation stability and does not require small relaxation coefficients. The SIMPLEC procedure, representing the core of the algorithm realized in the VP2/3 package, is not a unique procedure of solving the equations entering into the FLUENT package. In this package, the known procedure of calculating incompressible-fluid flows, based on the concept of artificial compressibility, is also used [16].

Selection of a computational model, namely, the relative position of nodes, at which discrete values of the desired parameters are determined, plays an important role in the construction of a computational algorithm and is determined in many respect by the interrelation between the velocity and pressure fields and their coordination. It is known [17] that the use of the so-called centered model, where all variables are connected to the centers of computational cells, i.e., to one and the same nodes, in combination with central-difference approximations of the pressure gradient, can lead to saw-tooth distributions of pressure and velocity. To avoid the appearance of such distributions, a staggered model with distributed nodes is introduced. In this model, the positions of discrete pressure values and scalar variables remain unchanged and the Cartesian velocity components are determined at the centers of the faces positioned, in uniform grids, at the centers between the centers of cells. This approach calls for the introduction of several control volumes for calculating dependent variables and, therefore, increases the volume of calculations, as compared with the case where the centered model is used.

The regulator proposed for the block of pressure correction by Rhie and Chow (see, e.g., [4, 16]) allows one to solve the problem of interrelation between the pressure and velocity with the use of a centered model. However, unlike the initial variant, the corrected flows are determined with a coefficient of 0.1 (calculated in numerical experiments in [4]). Such an approach is used in all packages, including the VP2/3 and FLUENT ones, even though, in the user's guide to the latter, no mention is made of the introduction of the indicated coefficient. A similar procedure of monotonization of the pressure field in a model with Cartesian velocity components positioned at the corners of computational cells was proposed by Chen; it is based on averaging of the mass defect in a cell over the mass defects in the neighboring cells [27]. This model is used in the preliminary UVP version of the VP2/3 package.

As was noted earlier, the problem of artificial diffusion (appearing in the 1980s), associated with approximation of convective terms in transfer equations, has been solved mainly due to the use of upwind schemes of the second order of accuracy, in particular Leonard's schemes with quadratic interpolation. It is precisely this scheme, more exactly its one-dimensional variant, that is used in the VP2/3 and FLUENT packages considered in the present work.

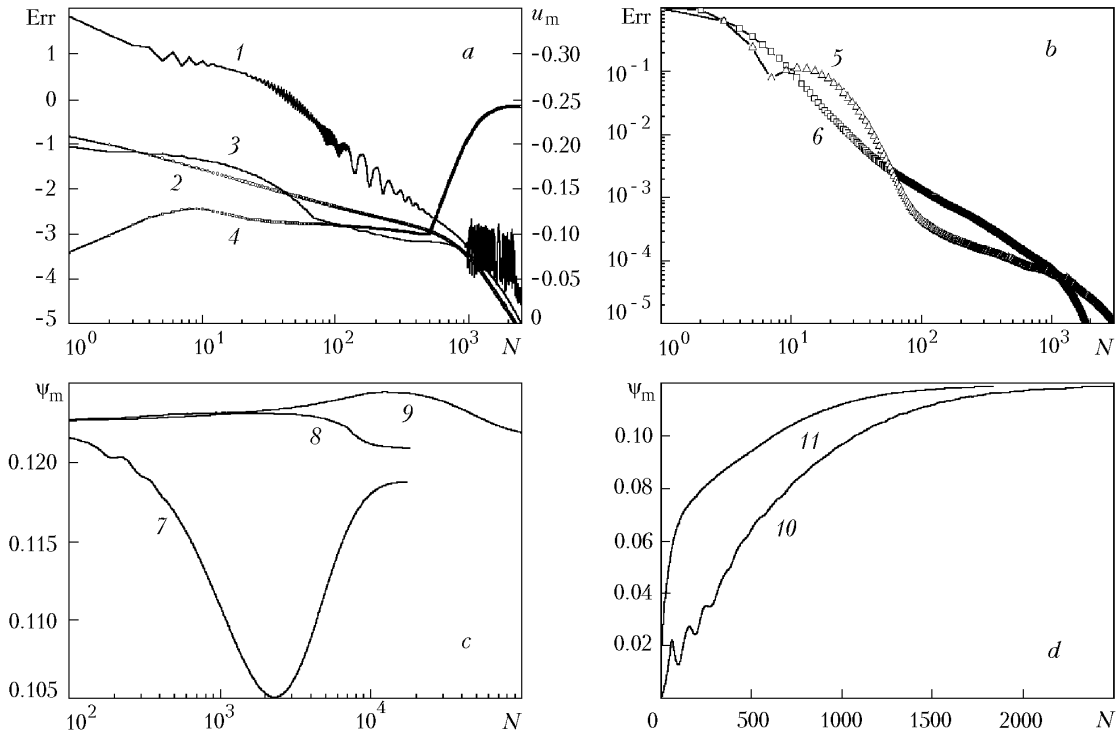

Fig. 3. Trajectories of convergence of the iteration processes of calculating circulation flows in a square cavity: a, b) behavior of the errors Err [1, 5, 6) δp; 2) δu; 3) δv] and local characteristics [4) u_m]; c, d) dependences ψ_m (7–11) for different Re [a) Re = 10^2 (1–4); b, d) 10^3 (6, 7, 10, 11); c) 10^3 (7), 10^4 (8), $2 \cdot 10^4$ (9)] and structured [a, b, d) 200 × 200; c) 400 × 400, curves 1–5, 7–10] and nonstructured [b, d) 200 × 200 curves 6, 11] grids and solvers [1–5, 7–10]) VP2; 6, 11) FLUENT].

The world's experience in practice in calculating stationary viscous-fluid flows at large Reynolds numbers with the use of discretization schemes of high orders of approximation points to the fact that, with these schemes, it is difficult to obtain a stable iteration-process convergence [16]; therefore, in the user's guide for the FLUENT package [5] it is recommended to use discretization schemes of the first order of accuracy and form initial approximations in the process of preliminary calculations at small Reynolds numbers. At the same time, the approach proposed for construction of the computational procedure in increments of dependent variables [4], realized in the VP2/3 package, is practically not sensitive to the choice of the scheme of discretization of convective terms in the explicit side of equations. It should be noted that, in the VP2/3 package, to increase the stability and the rate of convergence of iterations, the convective terms in the implicit side of equations are calculated on an upwind scheme with one-sided differences and the diffusion-transfer coefficient is multiplied by the constant parameter OTL (which is usually larger than unity) and is determined in numerical experiments, which makes it possible to smooth physical oscillations [21]. In both packages, a lower-relaxation coefficient (of the order of 0.3) is used for calculating the velocity components.

The efficiency of the computational process is essentially dependent on the choice of the method for solving algebraic equations. In the VP2/3 package, the procedure of incomplete factorization of matrix in the SIP variant of stone [8] is used for this purpose. In the investigations carried out with the FLUENT package, we used the Gauss–Seidel procedure in combination with an algebraic multigrid accelerator.

Testing of Packages. Estimation of the Influence of Scheme Parameters on the Solution. A circulation laminar flow of an incompressible fluid around a square cavity, initiated by the movement of one of the cavity boundaries (the upper boundary in this case), was calculated on structured and nonstructured grids with a nonuniform distribution of cells and a bunching to the walls around which the stream flows. In the classical separation flow considered, there arise various different-scalar structures representing boundary layers built up on the walls (with a thick-

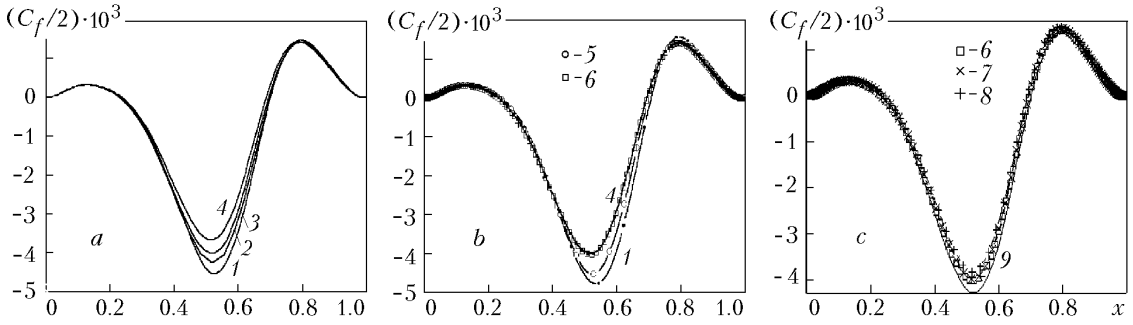

Fig. 4. Comparative analysis of the friction-coefficient distributions over the bottom of the cavity obtained on noncentered (1–4) grids with a different number of cells (a) with the use of noncentered and centered (5, 6) models (b) with a varying near-wall pitch δ_x (c). Grids 1, 5 contain 50 × 50; 2) 75 × 75; 3) 100 × 100; 4–8) 200 × 200; 9) 400 × 400 cells; 1–6) $\delta_x = \delta_y = 10^{-3}$; 7) $2\cdot10^{-4}$; 8) 10^{-4}; 9) 10^{-5}.

ness decreasing with increase in the Reynolds number), a primary vortex of scale equal to the characteristic size (a fin of the cavity), and secondary corner vortices, whose scales can differ from the scale of the primary vortex by an order of magnitude or more. To represent the above-indicated structures with an appropriate accuracy, it is necessary to impose fairly exacting requirements on the sizes of the computational cells, mainly on those in the near-wall and corner zones. This is largely true for the near-wall steps δ_x and δ_y.

As was already noted, structured and nonstructured grids are used for representation of both investigation objects and flows around them. Grids of the second type are mainly used in packages, since they are considered as more universal for calculating flows in regions with a complex geometry. Undoubtedly, comparative analysis of the results of simulation of separation flows even in simple regions is very useful for conclusions determining the applicability of different-topology grids. Figure 2 shows some of the grids considered. In the VP2/3 package, computational grids are constructed by an analytical method with a pitch increasing monotonically from the wall to the center of the cavity (Fig. 2a and b), and, in the FLUENT package (Fig. 2c and d), a computational grid consists of a central core with cells of the same size (square or triangular) and near-wall zones of thickness 0.003 filled with rectangular cells and has a pitch decreasing along the normal to the wall (δ_x and $\delta_y = 10^{-5}$).

The Reynolds number Re was determined by the velocity of travel of the upper boundary of the cavity U and by the length of the face L. The Re number was varied from 10^2 to $6\cdot10^4$.

Some of the methodical calculation materials are presented in Figs. 2–5 and in Table 1.

A typical iterative convergence, obtained in the process of simulation of a reverse flow around a cavity at Re = 10^2 with the use of the VP2/3 package, is illustrated in Fig. 3a. It is interesting to analyze the dependence of the maximum errors in dependent variables (pressure (1) and horizontal (2) and vertical (3) Cartesian velocity components) and the minimum longitudinal velocity of the flow in the first vortex (4) on the number of iterations N. A significant decrease in the errors (by several orders of magnitude) was obtained for a third of the iterations taking approximately one-half of the computational time at a practically constant velocity u_m. Only for the errors changing in the range 10^{-4}–10^{-5} did the intensity of the flow in the primary vortex and the maximum value of the stream function ψ_m increase monotonically and tend to an asymptotic value.

Figure 3b shows the trajectories of convergence of the iteration processes of solving the problem considered on structured and nonstructured grids at Re = 10^3 with the use of the FLUENT package. These trajectories are similar on the whole to the trajectories shown in Fig. 3a. It should be noted that the convergence is obtained more rapidly with a rectangular grid than with a triangular grid.

The influence of the pattern on similar structured grids ($\delta_x = \delta_y = 10^{-3}$) and the number of cells n distributed along the cavity boundary on the results of numerical calculations of a circulation flow in the case where the convergence criterion $|\delta u, \delta v| < 10^{-3}$ is fulfilled is shown in Table 1. It should be noted that, in the noncentered model used in the previous version of VP2/3, the nodes for the velocity components are positioned at the corners of a computational cell and the pressure is determined at its center, while the centered model is used in all of the subsequent ver-

TABLE 1. Influence of the Number of Computational Cells in a Square Region ($\delta_x = \delta_y = 10^{-3}$) on the Extremum Characteristics of a Flow around a Cavity at Re = 10^3

Type of model	$n \times n$	N_{it}	u_m	v_m	v_{max}	ψ_m
Noncentered	50×50	539	–0.365	–0.678	0.361	0.1113
	75×75	858	–0.382	–0.6793	0.3764	0.1165
	100×100	1208	–0.387	–0.6795	0.380	0.1180
	200×200	3666	–0.390	–0.680	0.3825	0.1189
	300×300	6779	–0.391	–0.680	0.383	0.1191
Centered	50×50	366	–0.3386	–0.6801	0.3544	0.1088
	75×75	719	–0.3817	–0.6798	0.3756	0.1163
	100×100	1194	–0.3876	–0.6796	0.3810	0.1185
	200×200	3609	–0.3901	–0.6796	0.3823	0.1191

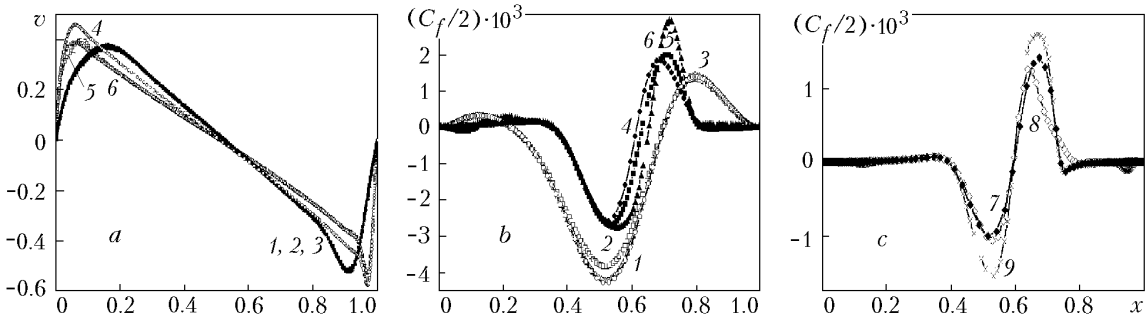

Fig. 5. Comparison of the profiles of the vertical velocity component in the horizontal middle cross section (a) and the friction-coefficient distributions over the cavity bottom (b, c) obtained for different Reynolds numbers [1–3) Re = 10^3; 4–6) 10^4; 7–9) $5 \cdot 10^4$) on structured (1, 2, 4, 5, 7–9) and nonstructured (3, 6) grids with the use of the VP2/3 (1, 4, 7, 8) and FLUENT (2, 3, 5, 6, 9) packages. All curves, except for curve 7, were obtained on 400 × 400 grids with a near-wall pitch of 10^{-5}; curve 7 was recalculated on a 200 × 200 grid with a near-wall pitch of 10^{-4}.

sions of VP2/3. First and foremost, in all of the models the results obtained with different grids converged, i.e., the integral and local characteristics of a flow stabilized with increase in the number of cells $n \times n$. As long as the convergence N_{it} is attained, the total number of iteration steps increases with increase in n, and, for coarse grids, the centered pattern is more preferential from the standpoint of computational efficiency. At the same time, the pattern of fine grids has no significant influence on the results of calculations.

As is seen from Fig. 3c, the rate of convergence of the iteration process of solving the problem decreases sharply with increase in the Re number; in this case, a decrease in the error cannot be considered as a reliable criterion of convergence. Therefore, the computational process was analyzed by the integral characteristic $\psi_m(N)$. At Re $> 10^4$, calculations were carried out beginning with the initial approximations, as which preliminary solutions obtained at other Reynolds numbers (which are not necessarily smaller) are used. For example, curve 7 in Fig. 3c, corresponding to Re = 10^3, was calculated at Re numbers beginning with Re = 10^4. At large Re, the convergence is attained on fairly fine grids for several tens of thousands of iteration steps.

Comparison of the dependences $\psi_m(N)$ (see Fig. 3d), obtained at Re = 10^3 on structured grids close in the number of cells with the use of different packages, shows that the FLUENT package provides a somewhat higher rate of convergence than the VP2/3 package. However, this can be due to the algebraic multiblock accelerator used in the first package.

Comparison of the distributions of the dimensionless friction over the cavity bottom, calculated using different models and grids different in density and near-wall step (Fig. 4), supports the conclusions made on the basis of the data presented in Table 1. In the case where economical grids with a noncentered pattern were used, the curves $C_f/2$ were separated (Fig. 4a). In this case, as is seen from Fig. 4b, the friction profiles calculated using different models are not coincident. At the same time, the distributions C_f obtained on identical fine grids (e.g., on 200 × 200 grids) are practically independent of them. A deformation of a structured grid, in the process of which the near-wall step decreases significantly (by an order of magnitude) down to 10^{-4} (Fig. 4c), is accompanied by an increase in the grid pitch in the central region of a cavity and leads to a insignificant decrease in the accuracy of the solution. For comparison, Fig. 4 shows the curve $C_f/2$ obtained using a 400 × 400 grid with a near-wall step $\delta_x = \delta_y = 10^{-5}$.

At the final stage of the methodical part of the work, the results of calculations performed at different Reynolds numbers on the finest rectangular and triangular grids with the use of the specialized and universal packages were compared (Fig. 5).

At Re = 10^3, the profiles of the vertical velocity component (Fig. 5a) in the horizontal middle cross section of the cavity, calculated on different grids, are practically coincident, while the distributions of the friction coefficient over the cavity bottom (Fig. 5b), calculated on a rectangular grid with the use of the FLUENT package, are somewhat different.

At Re = 10^4, the difference between the calculation data is much larger. Despite the acceptable agreement between the results obtained with the use of different packages, the velocity profile $v_{0.5}$ calculated on a rectangular grid with the use of the VP2/3 package differed from the other analogous velocity profiles. At the same time, the profiles $v_{0.5}(x)$ determined in the process of simulation of the flow considered on grids different in topology with the use of the FLUENT package were very close. By contrast, the friction distributions over the cavity bottom, calculated on structured grids, coincide well independently of the package used. The $C_f/2$ curves calculated on a triangular grid differ insignificantly from the analogous curves but only in the region of the secondary corner vortex. The maximum values of $C_f/2$ in the zone of the primary vortex, calculated on different grids with the use of different packages, are coincident.

At Re = $5 \cdot 10^4$ (Fig. 5c), the agreement between the results of calculations performed on different structured grids with the use of different packages seems to be wholly satisfactory. It should be noted that the distributions $C_f/2$ calculated on the 200 × 200 grid differed somewhat from those calculated on the 400 × 400 grid (curves 7 and 8).

Estimation of the Influence of the Reynolds Number. As was already noted, the present work is a continuation of the numerical investigations carried out in [6] for the case of large Reynolds numbers. The results obtained complement, correct, and develop the views of separation flows with numerous circulation zones. The calculations carried out on very fine grids were analyzed using mainly the VP2/3 package, even though they were compared with the calculations done with the use of the FLUENT package. Some of the results obtained are presented in Figs. 6–9 and in Tables 2 and 3.

The data presented in Fig. 6 and Tables 2 and 3 first of all characterize the primary vortex formed in a cavity, in which the extremum parameters of the flow and its integral characteristic — the stream function that is largest in magnitude in this structural formation — change with increase in Re. It is commonly supposed that the indicated data are most important for the separation flow considered since they make it possible not only to estimate the reliability of the numerical models used and supplement the accumulated statistical data but also to perform hydrodynamic analysis of the large-scale motion forming the flow as a whole. As is known, large vortices are simulated on the basis of such analysis. Since the results of calculations of a circulation flow in a cavity, which have been performed within the span of several decades, were analyzed in detail in [6], in the present work we dwell only on new results and compare forecasts obtained with the use of different program packages.

More than twenty-five years ago, one of the authors of the present article proposed to consider the integral parameter ψ_m characterizing the mass of the viscous fluid moving in a cavity as a criterion of the accuracy of numerical calculations (see, e.g., [8, 11, 13]). Evidently, as the ψ_m value, we should take a value limiting for monotonically bunching grids, which is easily estimated, in particular, from Table 1. However, in practice, a certain fairly fine grid is usually used. On this grid, a series of calculations is performed for increasing Reynolds numbers, and each subsequent calculation begins with the results of the previous calculation corresponding to a smaller Re number. This approach, illustrated in Table 2, is used partly in the present work. Nonetheless, the preliminary results obtained using

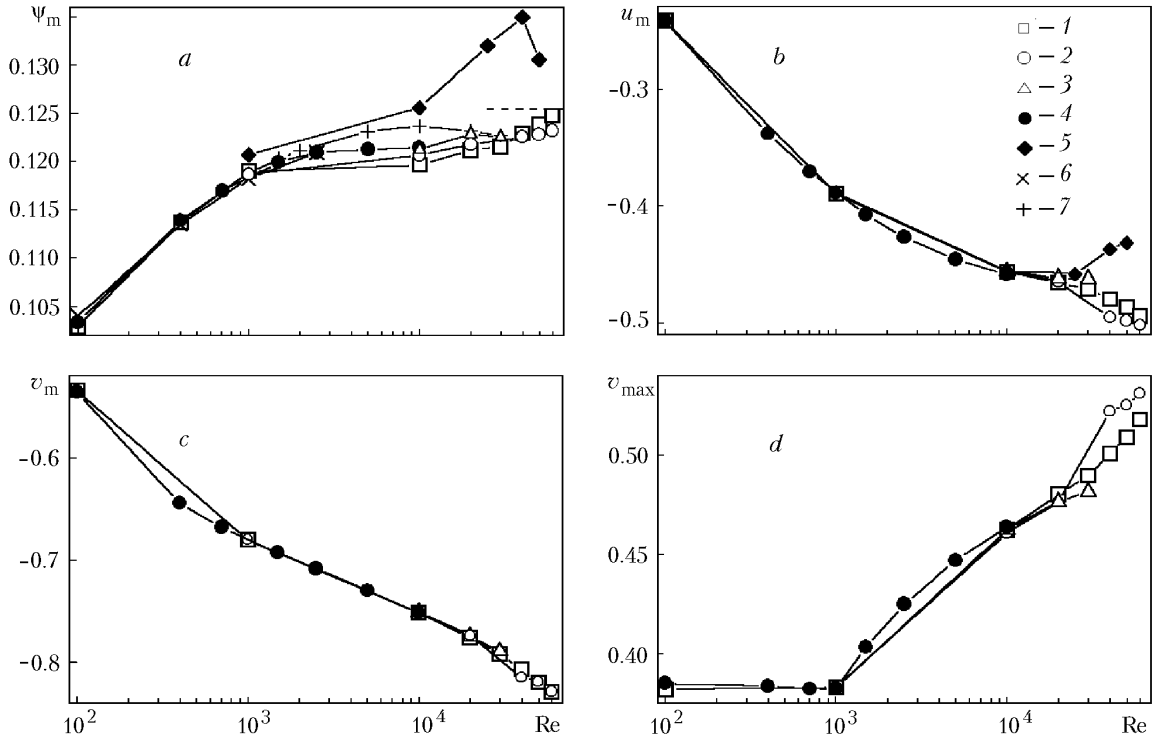

Fig. 6. Dependences of the minimum values of the stream function (a) and the horizontal (b) and vertical (c) velocity components and the maximum values of the vertical velocity component (d) on the Reynolds number obtained on different structured grids [1) 200 × 200, $\delta_x = 10^{-4}$, $\delta_y = 2\cdot10^{-5}$; 2) 400 × 400, $\delta_x = \delta_y = 10^{-5}$; 3) 200 × 200, $\delta_x = \delta_y = 10^{-4}$; 4) set of grids: 100 × 100; 200 × 200; 300 × 300; 400 × 400, $\delta_x = \delta_y = 10^{-5}$; 5) 400 × 400, $\delta_x = \delta_y = 10^{-5}$] and packages [1–4) VP2/3; 5) FLUENT]; dashed line) asymptotic value of ψ_m determined by Batchelor; 6) [11]; 7) [6].

the grids selected were found to be not entirely satisfactory and, therefore, they were then verified using a set of inset grids. As the initial grid, we used a grid containing 100 × 100 cells with a near-wall step of 10^{-5}. Of course, this grid is fairly coarse in the central region of the cavity and the solution obtained with it is very approximate. We successively refined the initial solution on finer 200 × 200, 300 × 300, and 400 × 400 grids with the same near-wall step; in this case, the solution was obtained on each grid using the initial approximation determined by interpolation on the previous grid. It is significant that a series of calculations on a set of grids was carried out at a fixed Reynolds number, i.e., Re remained unchanged when the density of the grids increased. The extremum values of the parameters of the flow at Re changing from 10^2 to 10^4 are presented in Table 3. It should be noted that they are obtained at OTL = 1, while all calculations of the flow at $\mathrm{Re} \geq 2\cdot10^4$ were performed at OTL > 1 (of the order of 10 and larger).

The results presented in Fig. 6 should be interpreted from two standpoints: (a) estimation of the accuracy of the forecasts and the applicability of the packages and (b) analysis of the transformation of a complex separation flow with increase in Re. As is known, the dependence $\psi_m(\mathrm{Re})$ should increase monotonically with increase in Re. A number of calculation data obtained on different grids with the use of the VP2/3 package support this conclusion. Unfortunately, the behavior of $\psi_m(\mathrm{Re})$ calculated on a structured grid (see Fig. 2c) with the use of the FLUENT package at large Re was different (Fig. 6a). An analogous situation was observed for the minimum longitudinal velocity u_m of the reverse flow in the middle cross section (Fig. 6b). In this case, the intensity of the flow in a large-scale vortex increased and the thickness of the boundary layer decreased with increase in Re. The forecasts made with the use of the FLUENT package do not correspond to the above-described behavior of $u_m(\mathrm{Re})$ at $\mathrm{Re} > 2.5\cdot10^4$, while the calculations carried out with the VP2/3 package correspond to it wholly satisfactorily.

TABLE 2. Influence of the Reynolds Number on the Extremum Characteristics of a Flow around a Cavity Calculated on Centered Grids

Grid parameters	Re	u_m	v_m	v_{max}	ψ_m
200×200 $\delta_x = 10^{-4}$ $\delta_y = 2\cdot10^{-5}$	10^2	–0.2419	–0.5341	0.3817	0.1029
	10^3	–0.3898	–0.6801	0.3830	0.1190
	10^4	–0.4566	–0.7513	0.4626	0.1197
	$2\cdot10^4$	–0.4656	–0.7759	0.4805	0.1212
	$3\cdot10^4$	–0.4710	–0.7921	0.4900	0.1216
	$4\cdot10^4$	–0.4795	–0.8068	0.5010	0.1230
	$5\cdot10^4$	–0.4867	–0.8197	0.5091	0.1239
	$6\cdot10^4$	–0.4944	–0.8289	0.5180	0.1248
400×400 $\delta_x = \delta_y = 10^{-5}$	10^3	–0.3894	–0.6798	0.3824	0.1187
	10^4	–0.4564	–0.6798	0.3824	0.1187
	$2\cdot10^4$	–0.4644	–0.7733	0.4767	0.1218
	$4\cdot10^4$	–0.4949	–0.8147	0.5221	0.1226
	$5\cdot10^4$	–0.4981	–0.8189	0.5255	0.1229
	$6\cdot10^4$	–0.5015	–0.8287	0.5312	0.1233

The disagreement between the data presented in Fig. 6a can be due to the influence of the quasistationary perturbations on the solution of the problem; these perturbations arise when stepwise initial conditions and very fine grids are used. This is especially true for the case where a circulation flow around a cavity is simulated with the FLUENT package, beginning with the state at which the fluid in the cavity is completely frozen. Somewhat smaller perturbations arise in the iteration process of solving the problem when the Re number changes. These perturbations cannot disappear rapidly in the case where fine grids are used. The process of dissipation of the excess vorticity caused by the quasinonstationary perturbations is extremely long, which leads to the above-indicated changes in ψ_m(Re).

The data presented in Table 3, which were obtained using a set of inset grids, show that the negative influence of the above-indicated quasinonstationary perturbations can be obviated. At moderate Reynolds numbers the convergence of data is attained even on a 200 × 200 grid. However, at large Re numbers the number of cells in a grid has a marked influence on the solution. It should also be noted that the quantities v_m and v_{max} depend on the grid used to a much lesser degree than the quantities u_m and ψ_m. This is explained, in all probability, by the fact that different-scale flows arise in a cavity with a mobile upper wall, i.e., the vertical scale influences a circulation flow much more substantially than the horizontal scale. Consequently, one may select a smaller near-wall pitch in the vertical direction as compared with the analogous pitch in the horizontal direction. This conclusion is supported by the data presented in Table 2.

Analysis of the graphs in logarithmic coordinates, presented in Fig. 6a, shows that they can be divided, with respect to the Re numbers, into three portions differing markedly in behavior. The first, markedly nonlinear portion corresponds to moderate Reynolds numbers of up to 10^3, at which the influence of the viscosity is dominant. The clearly defined portion of stabilization (at Re changing from 10^3 to 10^4) and the near-linear portion (at Re larger than 10^4) are formed under the dominant action of the forced convection.

The author's experience suggests that, at $Re \to \infty$, the behavior of the extremum characteristics of a flow around a cavity is asymptotic in character. This idea follows mainly from the fact that, in this case, the Batchelor hypothesis is fulfilled. According to this hypothesis, a limiting flow having a nonlinear core surrounded by a very thin boundary layer is formed in the cavity [8]. The present work supports, on the whole, the indicated hypothesis, even though distinct asymptotic values of ψ_m were not obtained at Re of the order of $5\cdot10^4$ (Fig. 6a).

The maximum absolute value of the horizontal velocity of the reverse flow changes approximately linearly at Re corresponding to the first and third intervals (in Fig. 6b). The corresponding curve experiences a deflection in the range of $Re = (1–2)\cdot10^4$.

TABLE 3. Influence of the Number of Computational Cells of Inset Centered Grids with a Minimum Near-Wall Pitch of 10^{-5} and the Reynolds Number on the Extremum Characteristics of a Flow around a Cavity

Re	$n \times n$	u_m	v_m	v_{max}	ψ_m
100	100×100	–0.2281	–0.5355	0.385	0.1009
	200×200	–0.2409	–0.5355	0.385	0.1032
	300×300	–0.2417	–0.5352	0.385	0.1033
	400×400	–0.2425	–0.5353	0.3851	0.1034
400	100×100	–0.3060	–0.6407	0.3835	0.1079
	200×200	–0.3341	–0.6435	0.3833	0.1131
	300×300	–0.3374	–0.6436	0.3834	0.1137
	400×400	–0.3381	–0.6436	0.3835	0.1139
700	100×100	–0.3412	–0.6672	0.3821	0.1099
	200×200	–0.3673	–0.6678	0.3821	0.1165
	300×300	–0.3703	–0.6674	0.3821	0.1169
	400×400	–0.3708	–0.6675	0.3822	0.1170
1500	100×100	–0.3808	–0.6945	0.3801	0.1135
	200×200	–0.4045	–0.6928	0.4011	0.1191
	300×300	–0.4073	–0.6927	0.4027	0.1198
	400×400	–0.4078	–0.6926	0.4033	0.1200
2500	100×100	–0.3960	–0.7103	0.3969	0.1130
	200×200	–0.4224	–0.7084	0.4215	0.1198
	300×300	–0.4262	–0.7080	0.4245	0.1207
	400×400	–0.4270	–0.7080	0.4251	0.1210
5000	100×100	–0.4052	–0.7319	0.4066	0.1115
	200×200	–0.4410	–0.7297	0.4427	0.1199
	300×300	–0.4452	–0.7295	0.4461	0.1209
	400×400	–0.4460	–0.7294	0.4471	0.1213
10 000	100×100	–0.4017	–0.7592	0.4018	0.1087
	150×150	–0.4396	–0.7541	0.4456	0.1171
	200×200	–0.4501	–0.7522	0.4573	0.1194
	300×300	–0.4564	–0.7515	0.4626	0.1208
	400×400	–0.4589	–0.7513	0.4641	0.1215

The maximum absolute value of the vertical velocity of the primary vortex in the region of the right wall at Re corresponding to the beginning of the first interval, at which the influence of the viscosity is dominant in the flow field, increases nonlinearly with increase in Re (Fig. 6c). Then a fairly large linear portion of $v_m(\mathrm{Re})$, corresponding to the second interval as well as the end of the first and the beginning of the third interval of change in Re, follows.

The behavior of the maximum vertical velocity of the flow in the neighborhood of the left wall at Re changing in the first interval seems to be somewhat paradoxical: v_{max} decreases slightly as Re approaches 10^3 and, in doing so, remains at a level of 0.38 (Fig. 6d). Then, at Re changing in the second interval, v_{max} increases sharply and changes with change in Re by a near-square law; in this case, v_{max} is practically equal to $|u_m|$.

The dependences of the extremum characteristics of a separation flow on Re, represented in logarithmic coordinates, remain near-linear at extremely high Re. It is interesting to consider the behavior of the extremum characteristics of a flow at Re of the order of $5 \cdot 10^4$ in the circumferential direction from the side wall positioned downstream of the flow to the bottom of the cavity and then to the side wall positioned upstream of the flow. Evi-

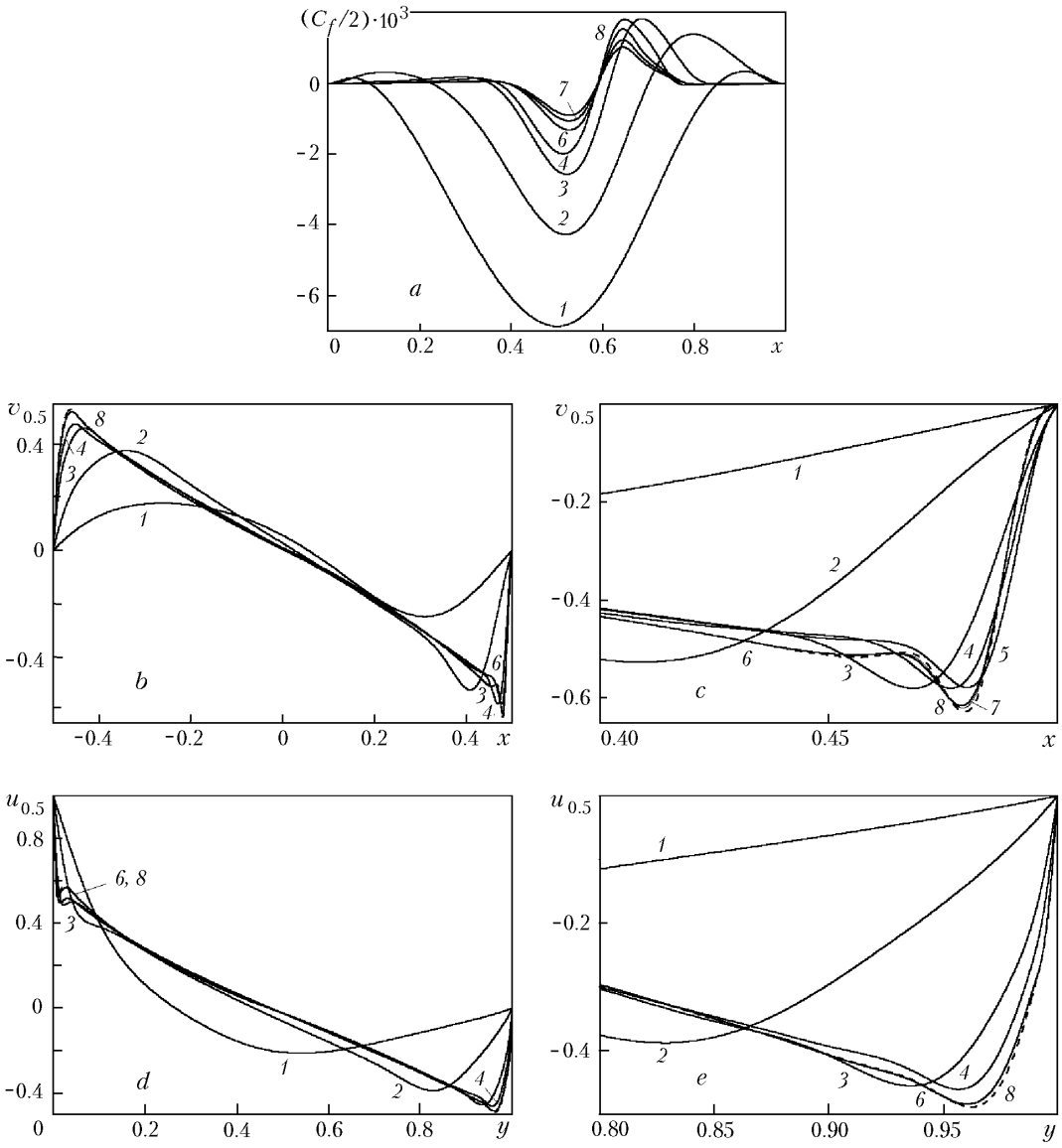

Fig. 7. Influence of the Reynolds number on the friction profiles at the bottom of the cavity (a), profiles of the vertical (b, c) and horizontal (d, e) velocity components in the middle cross sections of the cavity: 1) Re = 10^2; 2) 10^3; 3) 10^4; 4) $2\cdot10^4$; 5) $3\cdot10^4$; 6) $4\cdot10^4$; 7) $5\cdot10^4$; 8) $6\cdot10^4$.

dently this direction is coincident with the direction of the fluid flow in the primary vortex. The velocity in the near-wall layer behaves in the following way: 0.82, 0.50, 0.52, and so on, i.e., the maximum velocity of the primary vortex in the lower and left parts of the cavity equalizes. It should be noted that (see Table 2), at Re $\geq 10^4$, the velocity components $|u_m|$ and v_{max} change synchronously in the range 0.45–0.5, i.e., their deviation from U does not exceed 5%. Thus, all significant deformations of the primary vortex happen at Re changing from 10^2 to 10^4.

Figure 7 shows the evolution of the distributions of local characteristics of the cavity — the friction at the bottom and the Cartesian velocity components in the middle cross sections — with increase in Re. These dependences are usually used in investigating a fluid motion in a square cavity [8] and support, on the whole, the data obtained in earlier works. The interest in high Re numbers is illustrated by the enlarged portions of the velocity profiles of the flows near the right side and lower walls of the cavity.

It also follows from the friction distributions presented in Fig. 7a that the whole range of change in Re should be divided into three intervals: from 10^2 to 10^3, from 10^3 to 10^4, and values higher than 10^4. It is easily seen

that very intense secondary vortices develop at Re increasing within the first interval; in this case, tertiary vortices do not appear. At $Re > 10^3$, the secondary vortices begin to move from the sites of their initiation, i.e., there arise fairly weak tertiary vortices playing the role of buffers for the secondary vortices. The maximum friction in the secondary vortex continues to increase at Re changing in the second interval of change in Re and becomes approximately constant at $Re = 10^4$; in this case, the friction is maximum in the region of the primary vortex at the bottom of the cavity. Then, in the third interval of change in Re, where $Re > (1–2) \cdot 10^4$, the maximum friction decreases monotonically with increase in Re.

The deformation of the profiles of the Cartesian velocity components in the characteristic cross sections is maximum in the first interval of change in Re (Fig. 7b–e). At $Re = 10^2$, the action of the viscosity on the flow is so large that the whole fluid motion in the cavity experiences it. For example, the horizontal velocity reaches a maximum, equal to approximately 24% of U, at the center of the computational region. In this case, the profile of the vertical velocity in the middle horizontal cross section has two extrema (–0.53, 0.38) and indicates that the thickness of the viscous layer increases when passing from the right to the left side walls.

It is seen that, at $Re = 10^3$, the core of a near-constant vorticity with a near-linear velocity profile begins to form. At the boundary of the core, the Cartesian velocity components in the middle cross sections are equal respectively to 0.68, 0.39, and 0.38. This points to a significant increase in the velocity of the reverse flow in the cavity. In this case, thick boundary layers are formed on the walls. Clearly, the thickness of the boundary layer on the mobile wall is the smallest: it comprises 5% of the characteristic dimension L in the vertical middle cross section. Near the right side wall there arises a flow, similar to a jet flowing along a wall or a shear layer on a wall, with a new boundary layer increasing as the bottom of the cavity approaches. The thickness of the layer in the horizontal middle cross section comprises 10% of L. At the same time, the thickness of the boundary layers in the characteristic cross sections at the bottom and at the left side wall of the cavity is approximately equal to 18% of L. This indicates that the large-scale primary vortex at the left corner is close in shape to a cylindrical vortex.

The second interval of change in Re is characterized by the formation of a large-scale primary vortex that is practically independent of Re. It should be noted that, at $Re \geq 10^4$, the profiles of the Cartesian velocity components in the middle cross sections superimpose. However, it is seen that they are significantly transformed at Re changing in the second interval. This is explained by the fact that, at $Re = 10^4$, at the boundary of the core of a near-constant vorticity, the Cartesian velocity components in the middle cross sections are equal to, respectively, 0.75, 0.46, and 0.46 (see Table 2), i.e., the reverse flow in the cavity intensifies markedly. Not only do the extremum characteristics of the flow increase but also the thickness of the boundary layers decreases. Moreover, the evolution of the structure of the separation flow in the cavity with increase in Re leads to the appearance of regions where the velocity components of the flow in the near-wall layers behave nonmonotonically. Thus, the secondary vortex arising at the upper left corner is responsible for the appearance of a local dip on the dependence $u_{0.5}(y)$ in the neighborhood of the mobile wall (Fig. 7d).

The third interval of change in Re is associated with local changes in the flow in the near-wall and corner zones of the cavity. The separation flow changes with increase in Re, even though its structure, including the structure of small-scale vortices, remains practically unchanged, which leads to a change in the profiles of the velocity components of the flow in the middle cross sections of very thin layers. It is interesting that an increase in the velocity maxima with increase in Re, beginning with $Re = 4 \cdot 10^4$ (see Fig. 6 and Tables 2 and 3), leads to the appearance of deflections on the nonmonotone portions of the profiles $v_{0.5}(x)$ (curves 5 and 6 in Fig. 7c) and a preseparation behavior of $v_{0.5}(x)$. It is seen from Fig. 7e that the rate of decrease in the thickness of the boundary layer with increase in Re in the interval considered is much smaller than that at Re changing in the other intervals.

The evolution of a circulation flow around a square cavity was repeatedly analyzed in numerical investigations (see, e.g., [4, 6, 8, 11, 14, 15]), some of which were oriented to the study of such a flow at large Reynolds numbers. Undoubtedly, the use of fine 400×400 grids with a near-wall pitch of 10^{-5} makes it possible to refine models of vortex structures, especially the smallest of them, and to increase the range of Re. In the present work, we analyzed, first of all, the evolution of the secondary and tertiary vortices on the basis of a catalog of the calculated patterns of separation flows (Fig. 8).

As was already noted when the changes in the friction profiles at the bottom of the cavity and in the Cartesian velocity components in its middle cross sections were analyzed, a rapid intensification of the circulation flow

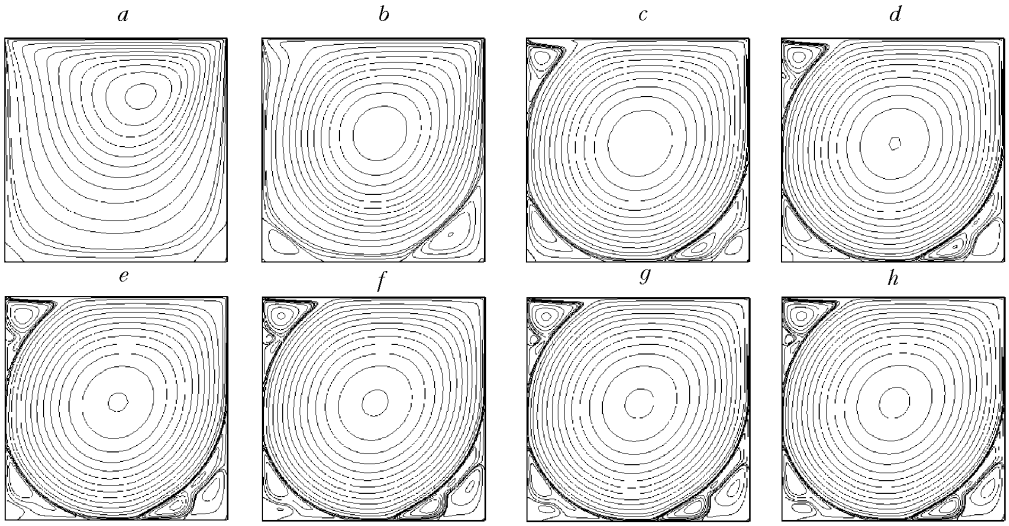

Fig. 8. Evolution of the pattern of a circulation flow in the cavity with increase in the Reynolds number: a) Re = 10^2; b) 10^3; c) 10^4; d) $2\cdot10^4$; e) $3\cdot10^4$; f) $4\cdot10^4$; g) $5\cdot10^4$; h) $6\cdot10^4$; the patterns represent lines of constant values of the stream function: –0.12, –0.11, –0.1, –0.09, –0.08, –0.07, –0.06, –0.05, –0.04, –0.03, –0.02, –0.01, –0.005, –0.001, –0.0005, –0.0001, 0, 0.0001, 0.0005, 0.001, 0.002, 0.003, 0.004, 0.005; the zero value is set on the wall, and the minimum value corresponds to the center of the primary vortex.

in the primary large-scale vortex with change in Re in the first interval is accompanied by the appearance of secondary corner vortices, whose size increases rapidly (at least by two times). It should be noted that the corner vortices play the role of distinctive guides for the flow in the primary vortex. Therefore, the so-called zero line of flow, separating the flows in the primary and secondary vortices, becomes more and more curved as Re increases (Fig. 8b).

At Re varying in the second interval (Re > 1200), there arises a secondary vortex at the upper left corner of the cavity. The reasons for its appearance were determined as early as the 1970s [11]; it is suggested that this vortex arises as a result of the deceleration of the reverse flow upstream of the upper boundary. It is interesting that the rapid decrease in the pressure of the flow at the upper left corner of the cavity, caused by the influence of the mobile wall, leads to the attachment of the flow to the side wall and the formation of a "suspension" corner separation zone stuck to the smooth wall. The dimensions of this zone and the intensity of the flow increase with increase in Re. In this case, the shape of the vortex at Re close to 10^4 becomes close to a triangle with curvilinear sides and smoothed angles (Fig. 8c).

It is interesting that, when the corner vortex at the left wall is not developed and an upper corner vortex is absent, the maximum vertical velocity of the first vortex remains unchanged. The development of the secondary vortices at the left wall leads to a rapid increase in v_{max}.

As was already noted, at large Reynolds numbers, the lower secondary vortices are forced from the corners and, in the immediate vicinity of them, there arise very weak but fairly lengthy tertiary vortices, though the left tertiary vortex is poorly defined at Re = 10^4. It should also be noted that the corner vortices are nonuniform in intensity. They include cores of constant vorticity that are shifted toward any wall of the cavity. For example, the vortex core of the right secondary vortex is shifted to the bottom, the core of the lower left secondary vortex is shifted to the left side wall, and the core of the upper left secondary vortex is positioned in the immediate vicinity of the mobile wall.

At Re varying in the third interval, the corner vortices consisting of secondary and tertiary vortex formations continue to grow. This is especially true for the upper left corner zone of the flow. Even at Re = $2\cdot10^4$, inside the secondary vortex on the wall there arises a tertiary vortex (Fig. 8d). The development of this vortex with increase in Re leads to a pinching of the internal circulation flow in this secondary vortex and its decomposition into a more intense vortex at the site of the former core and into a smaller-scale vortex. It should be noted that, at a certain instant of development of the new structure consisting of three vortices, a singular point belonging simultaneously to all three

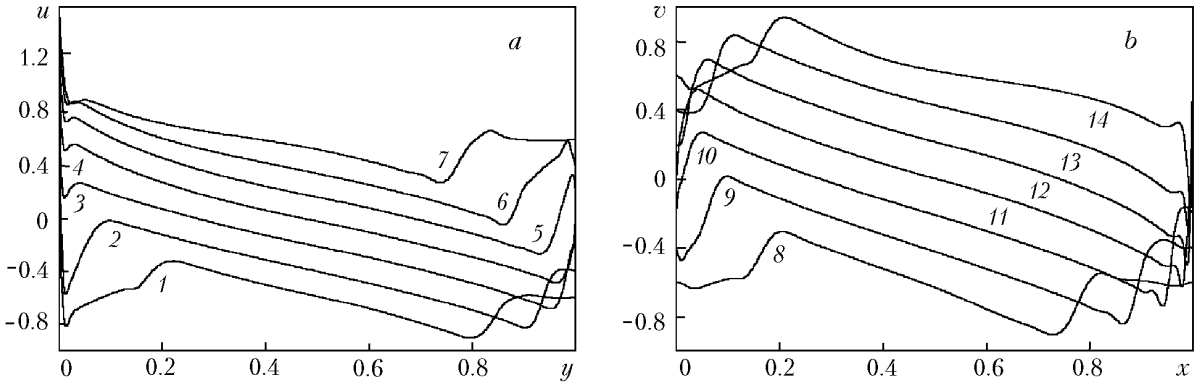

Fig. 9. Deformation of the profiles of the horizontal (a) and vertical (b) velocity components in the cavity at Re = $4 \cdot 10^4$: 1) x = –0.375; 2) –0.25; 3) –0.125; 4) 0; 5) 0.125; 6) 0.25; 7) 0.375; 8) y = –0.375; 9) –0.25; 10) –0.125; 11) 0; 12) 0.125; 13) 0.25; 14) 0.375.

vortices arises on the profile of the separation flow. As Re exceeds $3 \cdot 10^4$, the largest vortex in the separation zone considered intensifies markedly, even though at Re of the order of $5 \cdot 10^4$ the vortex structures formed in this zone (their sizes first of all) stabilize.

An increase in Re also significantly influences the evolution of the tertiary vortices at the lower corners of the cavity. As in the case of the upper separation zone, at Re $\geq 2 \cdot 10^4$ the intensification of the right tertiary vortex and an increase in its dimensions leads to the decomposition of the core of the neighboring secondary vortex. This effect also takes place in the lower left separation zone; in this case, unlike the upper left vortex, the lower tertiary vortex changes markedly and, in doing so, demonstrates that the Re number continues to influence the vortex structure of the flow as a whole in the cavity. This is also evidenced by the above-indicated transformation of the velocity profile in the middle cross sections, i.e., the corner separation zone continues to increase insignificantly but still markedly.

Undoubtedly, the Batchelor hypothesis should be considered when the asymptotic behavior (at Re $\to \infty$) of vortex structures in a cavity is analyzed. Of course, it is practically impossible to represent a vortex nonviscous-liquid motion in a square cavity, which would be connected to the walls of the cavity through a thin boundary layer, even though it is precisely this model that was considered by Burggraf [28] (the dashed line in Fig. 6a was constructed on the basis of his estimates). Without question, the Skvair model problem for a round cavity seems to be more justified. Nonetheless, the Batchelor hypothesis can be used for investigating a laminar circulation flow of a viscous fluid at high Reynolds numbers. As was already shown, the asymptotics of the dependence $\psi_m(\mathrm{Re})$ calculated at Re $\to \infty$ agrees well with the estimation of $\psi_{m\infty}$ made by Burggraf [28]. At the same time, the analysis of the structure of the flows presented in Fig. 8 shows that flows at large Re numbers (of the order of $5 \cdot 10^4$), excluding the flows in the zone of interaction of the shear layer accelerated by the mobile wall with the side wall, can have a vortex structure. In the other regions of a square cavity, a large-scale vortex is similar to a cylindrical vortex. In any event, this follows from the analysis of the configuration of the separating line of flow. It is also evident that the system of fairly intensely generated secondary and tertiary vortices will continue to develop at Re $\to \infty$.

Finally, it is interesting to analyze the deformations of the profiles of the Cartesian velocity components of flows at large Reynolds numbers in a number of cross sections of a cavity along the horizontal and vertical coordinates (Fig. 9). This analysis supports the assumptions that cores of constant vorticity are formed in the primary and secondary vortices. The nonmonotone behavior of the velocity-component profiles in both directions is easily explained by the existence of numerous local separation zones. The zones occupied by tertiary vortices are filled, in fact, with a decelerated fluid since the velocity of the flow in them is very small.

This work was carried out with financial support from the Russian Basic Research Foundation (project Nos. 04-02-81005, 02-02-17562, 02-01-00670, and 02-01-01160).

NOTATION

C_f, friction coefficient, i.e., friction stress related to the kinetic head, in fractions of $\rho U^2/2$; Err, increment of a dimensionless dependent variable; i, number of a processor; L, length of the side of a square cavity; n, number of cells of a grid along a coordinate; N, current number of an iteration; OTL, constant parameter of the diffusion-transfer coefficient; Re, Reynolds number (Re = UL/ν); x and y, horizontal and vertical coordinates, m; U, velocity of a uniform flow, m/sec; V, computational speed, Mflops; u and v, horizontal and vertical Cartesian velocity components in fractions of U; t, time, years; δu, δv, increments of Cartesian velocity components, in fractions of U; δp, increment of pressure related to the doubled kinetic head, in fractions of ρU^2; δ_x and δ_y, near-wall pitches of a grid along x and y respectively, in fractions of L; ν, kinematic viscosity, m^2/sec; ρ, density, kg/m^3; ψ, stream function; $|\ |$, absolute value. Subscripts: it, iterations, total number; m and max, minimum and maximum values; 0.5, parameters in the middle cross section; ∞, asymptotic value.

REFERENCES

1. S. A. Isaev, I. A. Pyshnyi, A. Yu. Snegirev, A. E. Usachov, and V. B. Kharchenko, in: G. A. Kryzhanovskii and E. A. Kuklev (Eds.), Multiblock computational technologies for solving fundamental, applied, and exploitation problems of power engineering and transport, *Nauch. Vestn. Akad. Grazhd. Aviats., Probl. Bezopasn. Ekspluat. Vozdushn. Transp.*, No. 1, 50–58 (2003).
2. W. Rodi, Simulation of turbulence in practical flow calculations, in: *Proc. Eur. Congr. on Computational Methods in Applied Sciences and Engineering*, 11–14 September 2000, Barcelona (2000), pp. 1–21.
3. A. D. Gosman, Developments in industrial computational fluid dynamics, *Trans. IChE*, **76**, Pt. A, No. 2, 153–161 (1998).
4. A. V. Ermishin and S. A. Isaev (Eds.), *Control of Flows around Bodies with Vortex Cells as Applied to Flying Vehicles of Integral Arrangement* (*Numerical and Physical Modeling*) [in Russian], MGU, Moscow (2003).
5. Fluent 6.1 User's Guide, Fluent Inc., Lebanon (2003).
6. S. A. Isaev, A. G. Sudakov, N. N. Luchko, and T. V. Sidorovich, Numerical simulation of a laminar circulation flow around a square cavity with a moving boundary at high Reynolds numbers, *Inzh.-Fiz. Zh.*, **75**, No. 1, 54–60 (2002).
7. P. J. Roache, *Computational Fluid Dynamics* [Russian translation], Mir, Moscow (1980).
8. I. A. Belov, S. A. Isaev, and V. A. Korobkov, *Problems and Methods of Calculation of Separation Incompressible-Fluid Flows* [in Russian], Sudostroenie, Leningrad (1989).
9. I. A. Belov and N. A. Kudryavtsev, *Heat Transfer and Resistance of Tube Bundles* [in Russian], Énergoatomizdat, Leningrad (1987).
10. I. A. Belov, I. P. Ginzburg, and S. A. Isaev, Motion and heat transfer in a closed region with moving boundaries, *Vestn. LGU*, No. 13, 41–50 (1976).
11. I. A. Belov and S. A. Isaev, Circulating liquid flow in a rectangular cavity at moderate and high Reynolds numbers, *Zh. Prikl. Tekh. Fiz.*, No. 1, 41–45 (1981).
12. L. G. Loitsyanskii, *Mechanics of Liquids and Gases* [in Russian], Moscow (1986).
13. S. A. Isaev and A. E. Usachov, Numerical simulation of separation flows in the problems of internal aerodynamics, *Prom. Aérodin.*, Issue 4 (36), 43–75, Mashinostroenie, Moscow (1991).
14. S. A. Isaev, P. A. Baranov, N. N. Luchko, T. V. Sidorovich, and D. P. Frolov, *Numerical Simulation of Separation Incompressible-Fluid Liquid Flow in Square and Cubic Cavities with a Moving Boundary* [in Russian], Preprint No. 7 of the A. V. Luikov Heat and Mass Transfer Institute, National Academy of Sciences of Belarus, Minsk (1999).
15. D. P. Frolov, *Identification of Spatial-Vortex Structures and Control of Flows with the Use of Vortex Cells* (*Numerical Simulation*), Author's Abstract of Candidate Dissertation (in Engineering), St. Petersburg (1999).
16. J. H. Ferziger and M. Peric, *Computation Methods for Fluid Dynamics*, 2nd ed., Springer–Verlag, Berlin–Heidelberg–New York (1999).
17. S. Patankar, *Numerical Methods for Solving Problems of Heat Transfer and Dynamics of Fluids* [Russian translation], Mir, Moscow (1984).

18. L. A. Dorfman, *Numerical Methods in Gas Dynamics of Turbines* [in Russian], Énergiya, Leningrad (1974).
19. G. Virts and Zh. Smoderen (Eds.), *Numerical Methods in Fluid Dynamics* [in Russian], Mir, Moscow (1981).
20. S. A. Isaev, A. I. Leont'ev, and A. E. Usachov, Methodological aspects of numerical simulation of the dynamics of vortex structures and heat transfer in viscous turbulent flows, *Izv. Ross. Akad. Nauk*, *Énergetika*, No. 4, 140–148 (1996).
21. S. A. Isaev, N. A. Kudryavtsev, and A. G. Sudakov, Numerical simulation of a turbulent incompressible viscous-fluid flow around bodies of curvilinear shape in the presence of a mobile shield, *Inzh.-Fiz. Zh.*, **71**, No. 4, 618–631 (1998).
22. P. A. Baranov, S. A. Isaev, Yu. S. Prigorodov, and A. G. Sudakov, Calculation of a laminar flow around a profile with passive and active vortex cells on multiblock intersecting grids, *Izv. Vyssh. Uchebn. Zaved.*, *Aviats. Tekh.*, No. 3, 30–35 (1999).
23. S. A. Isaev, A. I. Leont'ev, P. A. Baranov, Kh. T. Metov, and A. E. Usachov, Numerical analysis of the effect of the viscosity on the vortex dynamics in a laminar separation flow around a hole on a plane with allowance for its asymmetry, *Inzh.-Fiz. Zh.*, **74**, No. 2, 62–67 (2001).
24. S. A. Isaev, A. G. Sudakov, P. A. Baranov, and N. A. Kudryavtsev, Testing of a multiblock algorithm for calculating nonstationary laminar separation flows, *Inzh.-Fiz. Zh.*, **75**, No. 2, 28–35 (2002).
25. S. A. Isaev, I. A. Pyshnyi, A. E. Usachov, and V. B. Kharchenko, Verification of the multiblock computational technology in calculating laminar and turbulent flow around a spherical hole on a channel wall, *Inzh.-Fiz. Zh.*, **75**, No. 5, 122–124 (2002).
26. P. A. Baranov, S. A. Isaev, N. A. Kudryavtsev, and V. B. Kharchenko, Calculation of oscillations of a cylindrical pendulum in a cavity filled with a viscous fluid with the use of sliding multiblock grids, *Inzh.-Fiz. Zh.*, **76**, No. 5, 61–70 (2003).
27. Y. S. Chen, A numerical method for three-dimensional incompressible flows using nonorthogonal body-fitted coordinate systems, *AIAA Paper*, No. 1654 (1986).
28. O. R. Burggraf, Analytical and numerical studies of structure of steady separated flows, *J. Fluid Mech.*, **24**, Pt. 2, 113–151 (1966).